Effect of spectral sampling on the temporal coherence analysis of a broadband source in a SFG interferometer

Pascaline Darré,* Ludovic Szemendera, Ludovic Grossard, Laurent Delage, and François Reynaud

XLIM, Département Photonique, Université de Limoges, UMR CNRS 7252, 123 Av. Albert Thomas, 87060 Limoges CEDEX, France

*pascaline.darre@xlim.fr

Abstract: In the frame of sum frequency generation of a broadband infrared source, we aim to enlarge the converted bandwidth by using a pump frequency comb while keeping a high conversion efficiency. The nonlinear effects are simultaneously induced in the same nonlinear medium. In this paper, we investigate the spectral filtering effect on the temporal coherence behavior with a Mach-Zehnder interferometer using two pump lines. We show that joined effects of quasi-phase matching and spectral sampling lead to an original coherence behavior.

© 2015 Optical Society of America

OCIS codes: (030.1640) Coherence; (120.2650) Fringe analysis; (120.3180) Interferometry; (160.3730) Lithium niobate; (190.4223) Nonlinear wave mixing; (190.7220) Upconversion; (230.7370) Waveguides.

References and links

1. R. Boyd, " Infrared upconversion for astronomy," Opt. Eng. **16**, 563-568 (1977).
2. D. Ceus, F. Reynaud, J. Woillez, O. Lai, L. Delage, L. Grossard, R. Baudoin, J.-T. Gomes, L. Bouyeron, H. Herrmann, and W. Sohler, "Application of frequency conversion of starlight to high-resolution imaging interferometry. On-sky sensitivity test of a single arm of the interferometer," MNRAS **427**, 95–98 (2012).
3. L. Ma, O. Slattery, and X. Tang, " Single photon frequency up-conversion and its application," Phys. Rep. **521**, 69–94 (2012).
4. E. Diamanti, H. Takesue, T. Honjo, K. Inoue, and Y. Yamamoto, "Performance of various quantum-key-distribtion systems using 1.55-μm up-conversion single-photon detectors," Phys. Rev. B **72**, 052311 (2005).
5. F. Marsili, V.B. Verma, J.A. Stern, S. Harrington, A.E. Lita, T. Gerrits, I. Vayshenker, B. Baek, M.D. Shaw, R.P. Mirin, and S.W. Nam, " Detecting single infrared photons with 93 % system efficiency," Nature **7**, 210–214 (2013).
6. A. Restelli, J.C. Bienfang, and A.L. Migdall, "Single-photon detection efficiency up to 50 % at 1310 nm with an InGaAs/InP avalanche photodiode gated at 1.25 GHz," Appl. Phys. Lett. **102**, 141104 (2013).
7. C. Langrock, E. Diamanti, R.V. Roussev, Y. Yamamoto, and M.M. Fejer, "Highly efficient single-photon detection at communication wavelengths by use of upconversion in reverse-proton-exchanged periodically poled $LiNbO_3$ waveguides," Opt. Lett. **30**, 1725–1727 (2005).
8. R.W. Boyd, *Nonlinear Optics* (Academic, 2008).
9. M.M. Fejer, G.A. Magel, D.H. Jundt, and R.L. Byer, "Quasi-phase-matched second harmonic generation : tuning and tolerances," IEEE J. Quantum Electron. **28**, 2631–2654 (1992).
10. R.T. Thew, H. Zbinden, and N. Gisin, "Tunable upconversion photon detector," Appl. Phys. Lett. **93**, 071104 (2008).
11. L. Ma, J.C. Bienfang, O. Slattery, and X. Tang, "Up-conversion single-photon detector using multi-wavelength sampling techniques," Opt. Express **19**, 5470 (2011).

#244263 Received 3 Jul 2015; revised 20 Aug 2015; accepted 21 Aug 2015; published 21 Sep 2015
© 2015 OSA

12. J. Guillot, D. Ceus, S. Brustlein, L. Del Rio, A. Desfarges-Berthelemot, V. Kermene, L. Grossard, A. Tonello, L. Delage, and F. Reynaud, "Widely tunable sum-frequency generation in PPLN waveguide pumped by a multi-wavelength Yb-doped fiber laser," Opt. Commun. **283**, 442–446 (2010).
13. J.-T. Gomes, L. Grossard, D. Ceus, S. Vergnole, L. Delage, F. Reynaud, H. Herrmann, and W. Sohler, "Demonstration of a frequency spectral compression effect through an up-conversion interferometer," Opt. Express **21**, 3073–3082 (2013).
14. S. Wabnitz, A. Picozzi, A. Tonello, D. Modotto, and G. Millot, "Control of signal coherence in parametric frequency mixing with incoherent pumps: narrowband mid-infrared light generation by downconversion of broadband amplified spontaneous emission source at 1550 nm," J. Opt. Soc. Am. B **29**, 3128–3135 (2012).

1. Introduction

Infrared upconversion detectors find applications in many fields like astronomy [1, 2] or quantum communication systems [3, 4]. Especially, they are used in single-photon counting regime to detect low flux with the possibility to use the related efficient data processing. The hybrid detector associates the second order non-linear process of sum frequency generation (SFG) with an efficient detector such as a silicon avalanche photodiode. This device provides an alternative to direct detection in the near-infrared with cryocooled superconducting single-photon detectors [5] or with InGaAs/InP avalanche photodiodes requiring a gated-mode operation to reduce the afterpulsing impact [6] and having a low detection efficiency.

Periodically poled $LiNbO_3$ (PPLN) waveguide allows to achieve an SFG process with a high conversion efficiency [7]. The waveguide conversion bandwidth, also denoted spectral acceptance, is determined by the quasi-phase matching condition among the three frequency modes [8] and the narrow bandwidth of spectral acceptance acts as a frequency filter [9]. The goal of this study is to investigate the possibility to enlarge the spectral bandwidth analyzed by the upconversion detector. Different techniques have been developed to broaden the bandwidth of this detector [10–12].

In a previous article, our team has reported a technique related to this subject with an input signal composed of two different frequency lines and a doublet pump spectrum [13] where each line of the pump spectral doublet addresses a single line of the input spectral doublet. In this framework, we have demonstrated a spectral compression effect through the SFG process. This experimental demonstration followed a numerical demonstration proposed by Wabnitz & al. [14] proving a spectral compression phenomenon with a SFG process using a non-monochromatic pump source.

In this paper, we propose to pursue this study in high-flux regime with a large bandwidth source and a pump frequency comb limited at two frequency lines. Unlike our previous work where the SFG process occured only at exact quasi-phase matching, here each pump line converts an extended bandwidth in the infrared spectrum since SFG process can also occur with a slight phase mismatch. The spectral properties linked to the upconversion of a large bandwidth signal will be studied with a Mach-Zehnder interferometer where a PPLN waveguide is implemented on each arm.

2. Filtering effects in a PPLN crystal with a broadband source

2.1. Frequency upconversion with a monochromatic pump source

First and foremost, we consider the conversion of a coherent signal source by a monochromatic pump wave driving the SFG process in a PPLN waveguide, a second order non-linear medium. We will define respectively ν_s, ν_p the frequency of one spectral component of the large spectral bandwidth source and of the pump signal, and ν_c the frequency of the signal converted through the SFG process.

The upconversion process must satisfy the energy conversion law such that $\nu_c = \nu_s + \nu_p$.

#244263 Received 3 Jul 2015; revised 20 Aug 2015; accepted 21 Aug 2015; published 21 Sep 2015
© 2015 OSA

Besides, the conversion efficiency of this process strongly depends on the phase mismatch between the three interacting waves in the non-linear medium given by the following expression [8]

$$\Delta k = \frac{2\pi}{c}(n_s \cdot \nu_s + n_p \cdot \nu_p - n_c \cdot \nu_c - \frac{c}{\Lambda}), \tag{1}$$

where n_s, n_p and n_c are the refractive index of the fundamental modes associated to input, pump and converted signals respectively. Λ is the poling period of the PPLN waveguide and c is the speed of light in vacuum. The normalized conversion efficiency can be expressed

$$\eta(\nu_s, \nu_p) = \text{sinc}^2\left(\frac{\Delta k L}{2}\right), \tag{2}$$

where L is the PPLN length. Considering a constant pump frequency ν_p, the spectral acceptance $\Delta\nu_{s,acc}$ is defined by the full width at half maximum (FWHM) of the normalized efficiency main lobe. The frequency conversion can be considered as efficient over this spectral bandwidth. Thus using a monochromatic pump, the SFG process acts as a spectral filter on the input signal [9].

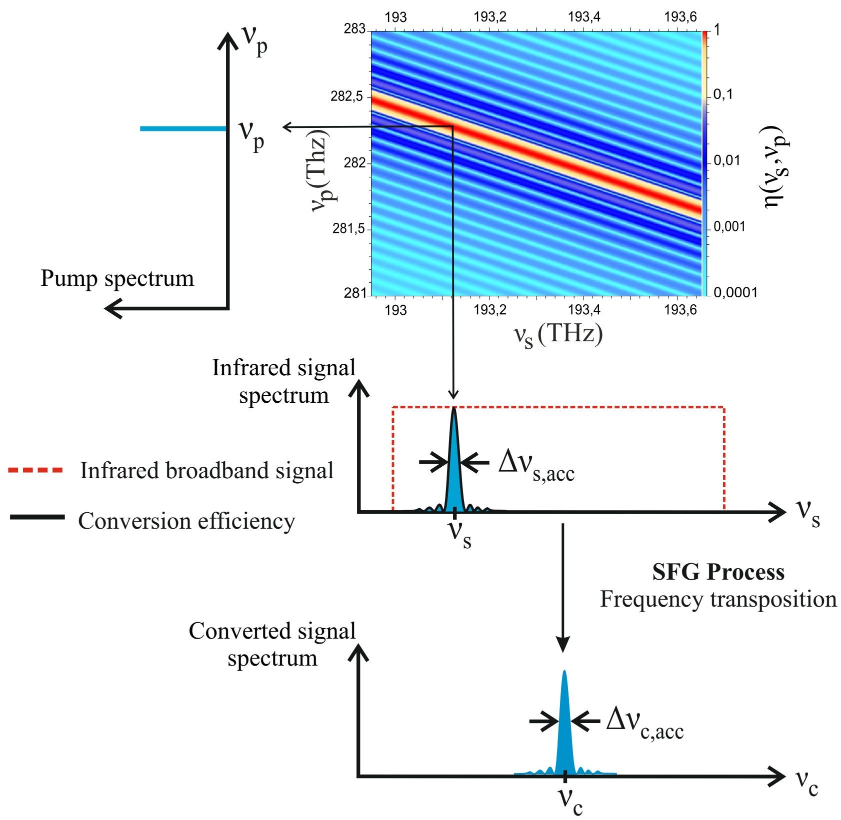

Fig. 1. Simulated color-map of the normalized sum frequency generation efficiency for different pump/signal couples. The red zone defines the maximum conversion efficiency. The phase-matching curve is retrieved by an orthogonal projection. The converted sample is represented below and corresponds to a frequency transposition of the infrared sample in visible domain.

The quasi-phase matching (i.e. $\Delta k = 0$) is obtained for a given set of signal and pump frequencies depending on the crystal parameters (i.e. poling period and operating temperature).

#244263 Received 3 Jul 2015; revised 20 Aug 2015; accepted 21 Aug 2015; published 21 Sep 2015
© 2015 OSA

We use a 22-mm-long PPLN waveguide. Figure 1 shows a color-map of the normalized conversion efficiency for different signal/pump couples simulated with our crystal parameters. The red zone corresponds to the maximum conversion efficiency over the frequency range probed in our study and gives the signal frequency associated to this maximum for a given pump frequency. We retrieve the curve defined by Eq. (2) with an orthogonal projection on the color-map. For instance with a pump signal at $\nu_p = 281.76$ THz (1064 nm) the red curve defines the maximum conversion efficiency at $\nu_s = 193.23$ THz (1551.5 nm). Considering a large signal bandwidth as input signal, this latter will be converted to the visible domain with a frequency spectral acceptance equal to $\Delta\nu_{s,acc} = 74.7$ GHz corresponding to 0.6 nm. The converted frequency, not represented on the map, can be deduced from the energy conversion law.

The frequency window considered through spectral filtering is defined by the spectral acceptance $\Delta\nu_{s,acc}$ of the input signal. Due to the energy conservation law, the converted spectral acceptance is preserved such as $\Delta\nu_{c,acc} = \Delta\nu_{s,acc} = \Delta\nu_{acc}$. Therefore the frequency conversion merely transposes the infrared spectrum to the visible domain through the SFG process.

As a consequence the upconversion of the broadband source is spectrally limited by the quasi-phase-matching condition in the PPLN waveguide. Thus reducing the crystal length would enable to increase the converted band. However the conversion efficiency increases with the square of crystal length [9]. To avoid a tradeoff between broadband response and conversion efficiency, we propose to enlarge the pump spectrum by using a frequency comb.

2.2. *Frequency upconversion with a frequency comb as pump source*

With a multi-pump source, each independent CW laser line converts different spectral samples centered on the frequencies ν_{s_i} defined by the maximal efficiency region (red zone in the color-map of Fig. 2). This leads to a spectral sampling of the broadband signal source. To optimize the converted spectral bandwidth, the lines of the frequency comb must be as close together as possible. However, a minimal spectral distance (a few $\Delta\nu_{acc}$) between them is necessary to avoid crosstalk between the different SFG processes taking place simultaneously in the nonlinear crystal.

In the following, we will consider only two incoherent pump laser lines as represented on Fig. 2. Accordingly, two independent nonlinear processes are generated simultaneously in the PPLN crystal and, on the frequency range scanned in our study, the red zone intercepted between the two points can be fitted by a linear function

$$\nu_p = a + b\nu_s. \tag{3}$$

The slope b only depends on the nonlinear medium dispersion properties. By substituting ν_p in the energy conservation law, this latter becomes

$$\nu_c = a + (1+b)\nu_s. \tag{4}$$

Thus the spectral width $\Delta\nu_c$ is written

$$\Delta\nu_c = (1+b)\Delta\nu_s, \tag{5}$$

where $\Delta\nu_i =\mid \nu_{i_1} - \nu_{i_2} \mid$ corresponds to the interval between two signal (i = s) or two converted (i = c) mean frequencies. Equation (5) indicates that a compression effect appears when two signal frequencies are transposed to the visible domain [13]. However the sample widths $\Delta\nu_{acc}$ are not affected by the compression effect as related to one monochromatic pump. This spectral compression only acts on the gap between the spectral samples. We define the spectral compression factor as

$$\rho = \tfrac{\Delta\nu_s}{\Delta\nu_c} = \left|\frac{1}{1+b}\right|. \tag{6}$$

#244263 Received 3 Jul 2015; revised 20 Aug 2015; accepted 21 Aug 2015; published 21 Sep 2015
© 2015 OSA

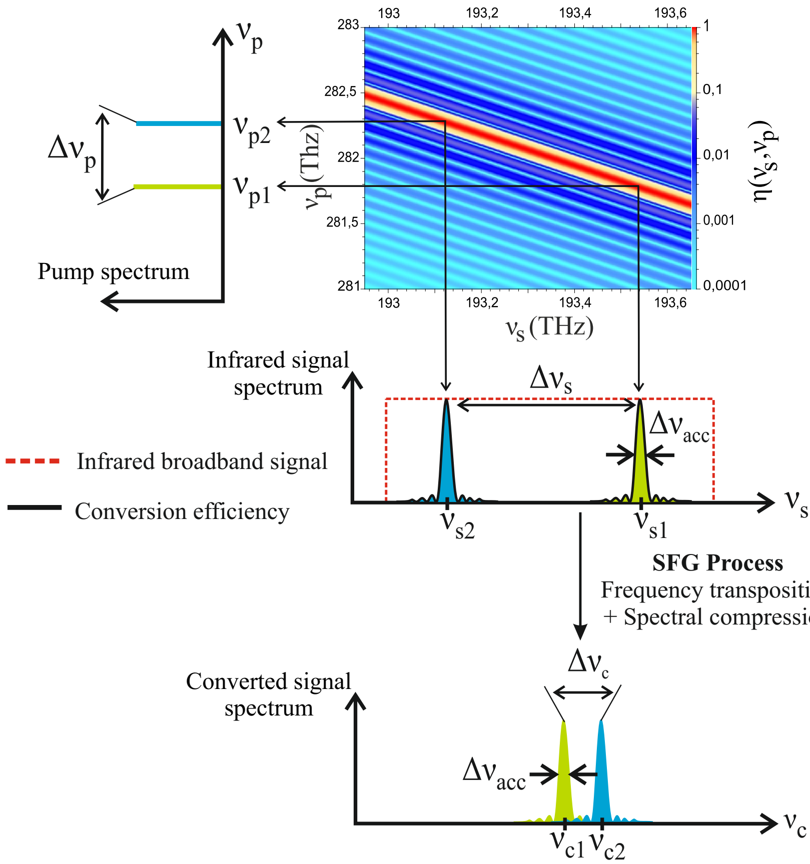

Fig. 2. Schematic representation of the spectral sampling of a large bandwidth source with a frequency comb of two laser lines (schema not to scale). For a given pump laser line, the color-map defines the spectral components ν_s converted by SFG on the broadband spectrum.

The slope of the red curve in the color-map gives $b_{num} = -1.2$ leading to a spectral compression factor $\rho_{num} = 4.8$. Notice that with one monochromatic pump the spectral compression effect is not meaningful since the red zone is only intercepted at one point. In the following, we propose to pursue the study by analyzing the spectral properties through an experimental approach using a Mach-Zehnder interferometer.

3. Demonstration of the spectral compression effect using temporal coherence analysis

3.1. *Method*

The spectral compression effect on the converted signal needs to be experimentally investigated with a high spectral resolution out of reach of a commercial spectrometer. To overcome the spectral resolution limitations of standard spectrometers, we propose to perform a temporal coherence analysis using an upconversion interferometer. The general architecture corresponds to a Mach-Zehnder interferometer including delay lines before and after the upconversion stage as indicated on Fig. 3. The interferometric signal obtained for one spectral component ν_s and

#244263 Received 3 Jul 2015; revised 20 Aug 2015; accepted 21 Aug 2015; published 21 Sep 2015
© 2015 OSA

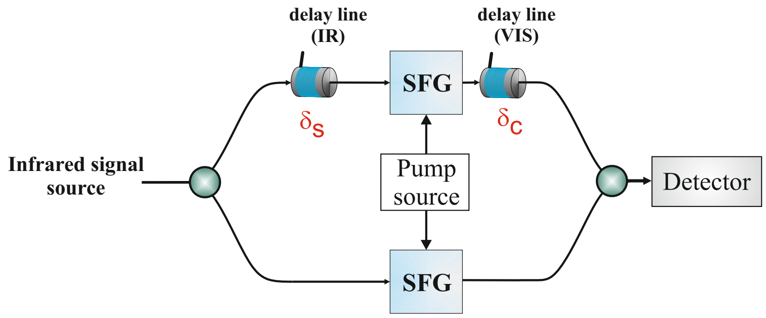

Fig. 3. Schematic layout of the Mach-Zehnder interferometer with the delay line before and after the sum frequency generation process. The delay can be applied either on infrared or on visible stage.

one pump line ν_p is expressed as

$$dI(\nu) \propto \Re\left(B(\nu)\left\{1+\exp\left[i2\pi\left(\frac{\delta_s\nu_s}{c}+\frac{\delta_c\nu_c}{c}\right)\right]\right\}d\nu\right), \tag{7}$$

with B(ν) the power spectral density (PSD), inferred from Eq. (2), and δ_i the optical path difference (OPD) between the two arms of the interferometer. This relation takes the phase terms on the infrared and the visible parts into account. As the frequency conversion takes place in the two arms, the OPD can be applied either on the infrared part or on the converted one. The resultant fringe system is computed all over the spectral components converted by one pump, either on the infrared or on the visible frequencies. The incoherent superposition of fringe systems associated to pump lines allows to rewrite the previous expression as

$$I(\nu) = \sum_k \Re\left(\int B(\nu)\left\{1+\exp\left[i2\pi\left(\frac{\delta_s\nu_s}{c}+\frac{\delta_c\nu_c}{c}\right)\right]\right\}d\nu\right), \tag{8}$$

with k the pump laser line index. Consequently Eq. (8) shows that the coherence analysis is twofold: the interferometer acts as an infrared correlator if an OPD variation is induced in the infrared delay line, and a visible one if the visible delay line is actuated. In the following sections, we will focus on the two coherence behavior analysis.

3.2. Coherence behavior with a single line pump

First consider the basic case of one pump source as presented on the Fig. 4 schematically illustrating the Mach-Zender interferometer and the signal detection. The infrared input signal is converted by SFG with only one pump line, and as detailed in section 2.1, the spectrum is simply shifted from infrared to visible frequencies. According to the Wiener-Khinchin theorem, the fringe contrast is given by the modulus of the PSD Fourier Transform

$$C(\delta) = \left|\text{Triangle}\left(\frac{\delta\Delta\nu_{acc}}{\pi c}\right)\right|. \tag{9}$$

According to Eq. (9), the fringe contrast plotted in Fig. 5 is a triangle function with identical characteristics in infrared and visible domains.

3.3. Coherence behavior with a dual-line pump source

In this configuration, the broadband source is sampled by a dual-line pump source. As two SFG processes are involved simultaneously on each interferometric arm, the related PSD of the

#244263 Received 3 Jul 2015; revised 20 Aug 2015; accepted 21 Aug 2015; published 21 Sep 2015
© 2015 OSA

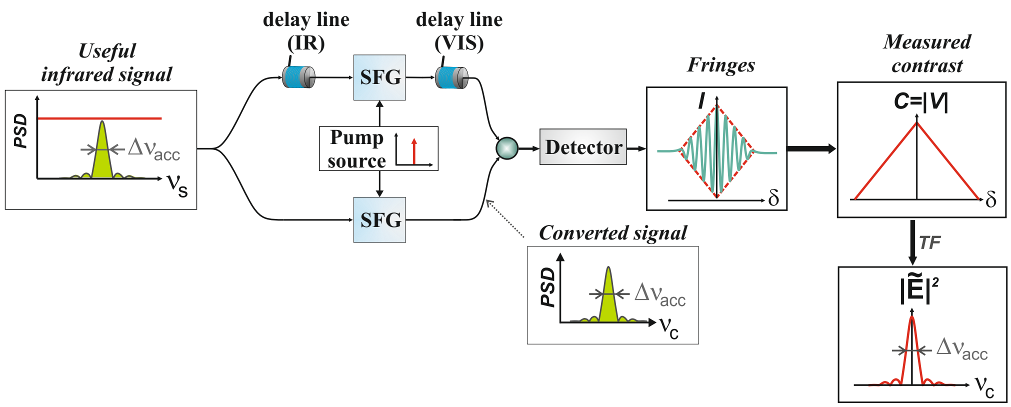

Fig. 4. Schematic layout with detection part for a single pump line. The Fourier Transform of the infrared or converted power spectral density (PSD) is analyzed by applying an OPD before or after the SFG process.

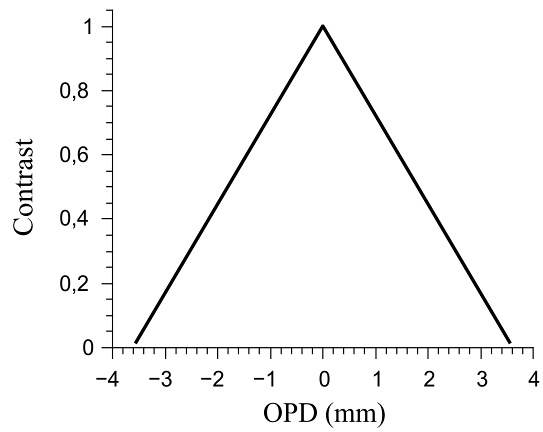

Fig. 5. Theoretical visibility obtained with a single-line pump.

useful infrared signal is written as

$$B(\nu) \propto \mathrm{sinc}^2\left(\frac{\pi(\nu-\nu_{s_1})}{\Delta\nu_{acc}}\right) + \mathrm{sinc}^2\left(\frac{\pi(\nu-\nu_{s_2})}{\Delta\nu_{acc}}\right). \tag{10}$$

Scanning the infrared delay leads to a temporal coherence analysis in the infrared domain (Fig. 6). According to the Wiener-Khinchin theorem, the fringe contrast can be expressed as a function of the infrared OPD δ_s

$$C(\delta_s) = \left|\mathrm{Triangle}\left(\frac{\delta_s\Delta\nu_{acc}}{\pi c}\right)\cos\left(\frac{\pi\delta_s}{c}\Delta\nu_s\right)\right|. \tag{11}$$

Equation (11) shows that the triangle function associated to the PPLN crystals is modulated by a cosine term with a periodicity depending on the infrared spectral spacing $\Delta\nu_s$. If the delay is applied after the SFG process, the interferometer acts as a visible correlator (Fig. 7). The fringe contrast is now written as

$$C(\delta_c) = \left|\mathrm{Triangle}\left(\frac{\delta_c\Delta\nu_{acc}}{\pi c}\right)\cos\left(\frac{\pi\delta_c}{c}\Delta\nu_c\right)\right|, \tag{12}$$

#244263 Received 3 Jul 2015; revised 20 Aug 2015; accepted 21 Aug 2015; published 21 Sep 2015
© 2015 OSA

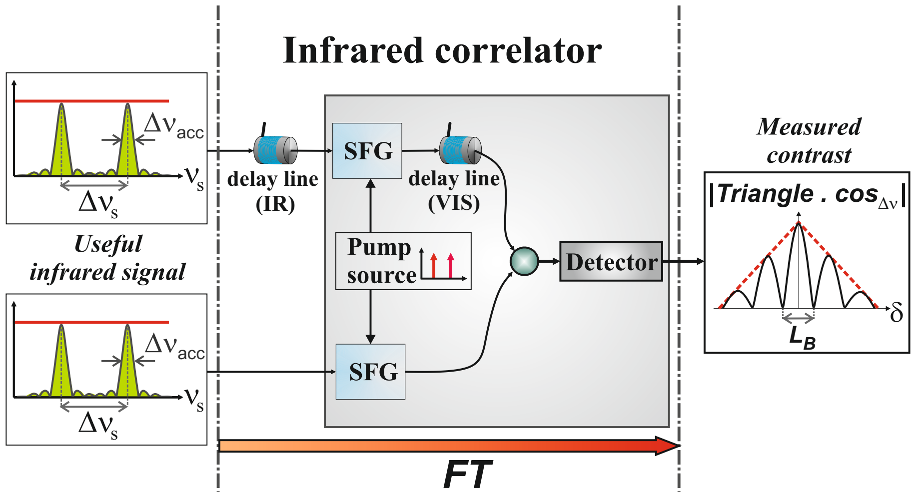

Fig. 6. Schematic layout of our experiment presented as an infrared correlator. The useful part of the infrared signal selected for the upconversion process is represented on each arm of the interferometer. As a delay is only applied on the infrared stage, the setup achieves the correlation between two infrared signals.

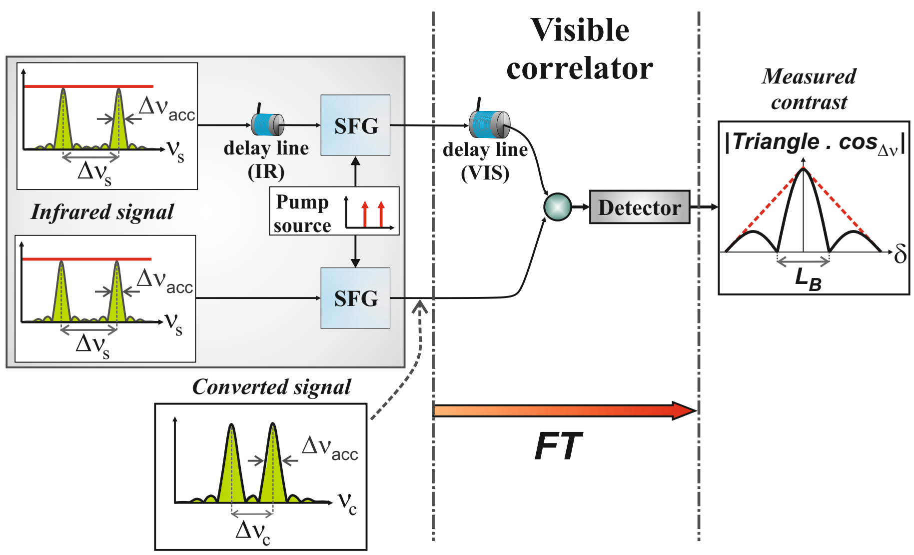

Fig. 7. Schematic layout of a visible correlator. A delay is applied on the visible stage which is the same as correlating two visible signals.

#244263 Received 3 Jul 2015; revised 20 Aug 2015; accepted 21 Aug 2015; published 21 Sep 2015
© 2015 OSA

where δ_c is the OPD applied on the visible stage. In the two expressions Eq. (11) and Eq. (12), the triangular envelope is identical while the cosine periodicity is different. We define the beat length $L_B = c/\Delta\nu$ as the half-period of the cosine associated with each expression. This way, the spectral compression factor can be expressed as the ratio of the beat length

$$\rho = \frac{L_{B_{VIS}}}{L_{B_{IR}}}. \tag{13}$$

In the next paragraph, we experimentally investigate the behavior of the fringe contrast evolution when scanning the visible or the infrared OPD.

4. Experimental demonstration of the spectral compression effect

4.1. Implementation of the SFG interferometer

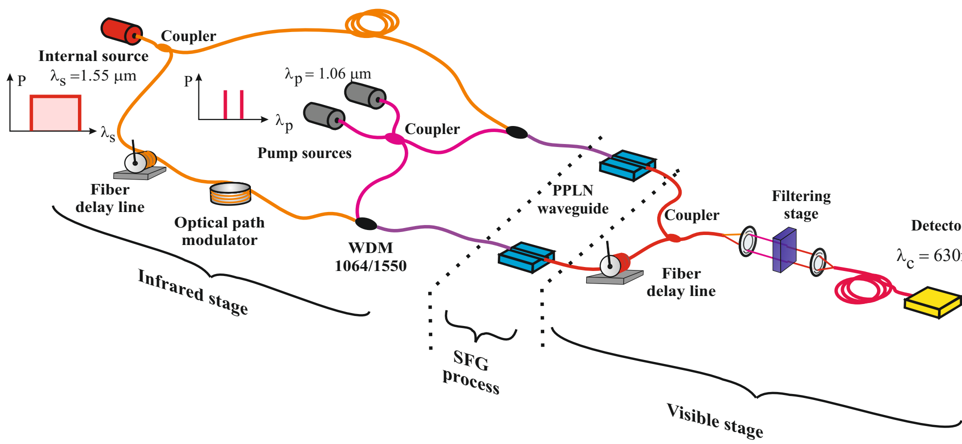

Fig. 8. Schematic layout of the experimental setup with a dual-line pump. Two upconversion processes are realized on each arm of the interferometer.

The experimental setup is based on a Mach-Zehnder interferometer as shown on Fig. 8. The pump spectrum is composed of a set of two independent distributed-feedback laser lines balanced in power and with a tunable spectral spacing. A pump line is fixed at $\nu_{p1} = 281.76$ THz ($\lambda_{p1} = 1064.0$ nm) and the second one ν_{p2} is tunable between 282.16 THz ($\lambda_{p2} = 1062.5$ nm) and 281.89 THz ($\lambda_{p2} = 1063.5$ nm). The infrared source is a superluminescent diode (SLED) with a bandwidth of about $\Delta\nu = 5$ THz ($\Delta\lambda = 40$ nm) centered at 194.17 THz ($\lambda = 1544.0$ nm) allowing to work with a temporally incoherent source. The PPLN temperatures are adjusted to have an efficient quasi-phase matching into the medium and two similar processes on each arm of the interferometer. Each pump line converts an infrared sample centered at a carrier frequency with a bandwidth of $\Delta\nu_{acc} = 74.7$ GHz (0.6 nm).

The input IR signal and the pump signal are equally shared between the two arms of the interferometer with a 50/50 fiber coupler. The experimental setup is almost entirely fibered with polarization maintaining and single-mode fibers. We inserted a fiber delay line of about 12-cm stroke on one arm of the interferometer in both visible and infrared stages. This delay line allows to control the OPD between the two arms on the infrared and the visible stages. An optical path modulator (OPM) with a 100-µm stroke is inserted on one arm of the interferometer on the infrared stage to induce a temporal optical path modulation to display fringe pattern as a function of time. The OPM is driven by a triangular high voltage to induce sequenced linear OPD scans.

#244263 Received 3 Jul 2015; revised 20 Aug 2015; accepted 21 Aug 2015; published 21 Sep 2015
© 2015 OSA

We use a wavelength-division multiplexing (WDM) to mix the signal and the pump with a polarization maintaining multiplexer before the SFG stage. The PPLN crystals are fibered and pigtailed at input and output faces. The multiplexed beam is sent through the SFG stage. The upconverted signals around 475.86 THz (630 nm) are recombined through a 50/50 fiber coupler. The outgoing interferometric signal is spectrally cleaned by a filtering stage composed of bandpass filters centered on the mean converted wavelength and a 7-m single-mode fiber allowing to remove pump residuals. The fringe pattern is then detected by a silicon photodiode.

4.2. Experimental results

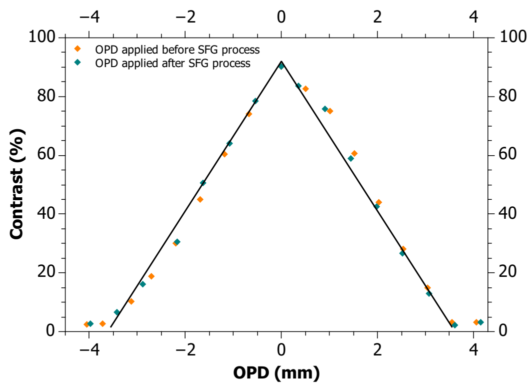

Fig. 9. Superposition of experimental fringe contrast obtained with one pump line and by applying an OPD before and after the SFG and comparison with the theoretical fit (black curve).

The first experimental investigation is realized with one monochromatic pump as described in section 3.2. By measuring the fringe contrast evolution of the upconverted signals as a function of the OPD between the two arms before and after the SFG process (Fig. 9), we demonstrate that our experimental results agree with the behavior predicted by the Wiener-Khinchin theorem. The fringe contrast evolution obtained by actuating the delay line before or after the upconversion process can be fitted by the same triangle function. As expected, no frequency spectral compression is observed with a single line pump. The fringe contrast is determined from the minimum and maximum intensities of the fringe pattern and, at the zero OPD, we obtained a maximum contrast value equal to 91.2 % probably due to polarization control defect in the interferometer.

In a second step, the SFG interferometer is powered by two laser lines as a pump source. Figure 10 shows the fringe contrast evolution by scanning the OPD on the two stages for different frequency gaps between the two pump lines.

As predicted by Eq. (11) and Eq. (12), a beat phenomenon modulates the triangular envelope related to the spectral acceptance $\Delta\nu_{acc}$ (see section 2.1). This latter is preserved even with two pumps and regardless of the difference $\Delta\nu_p$ between pump frequencies. Similarly, we retrieve the same maximum contrast value at the zero OPD as with one monochromatic pump. We can notice that the beat periodicity decreases with the frequency spacing $\Delta\nu_p$ and the beat length is higher when the OPD is applied on the visible stage.

Table 1 sums up the spectral compression factor obtained from Eq. (13) for different values of $\Delta\nu_p$. For each value, we give the relative experimental error compared to the simulated compression factor of 4.8. Fitting the visible contrast with Eq. (12) is awkward since beats are fewer than in infrared domain. Consequently fit parameters related to the cosine term introduce a sig-

#244263 Received 3 Jul 2015; revised 20 Aug 2015; accepted 21 Aug 2015; published 21 Sep 2015
© 2015 OSA

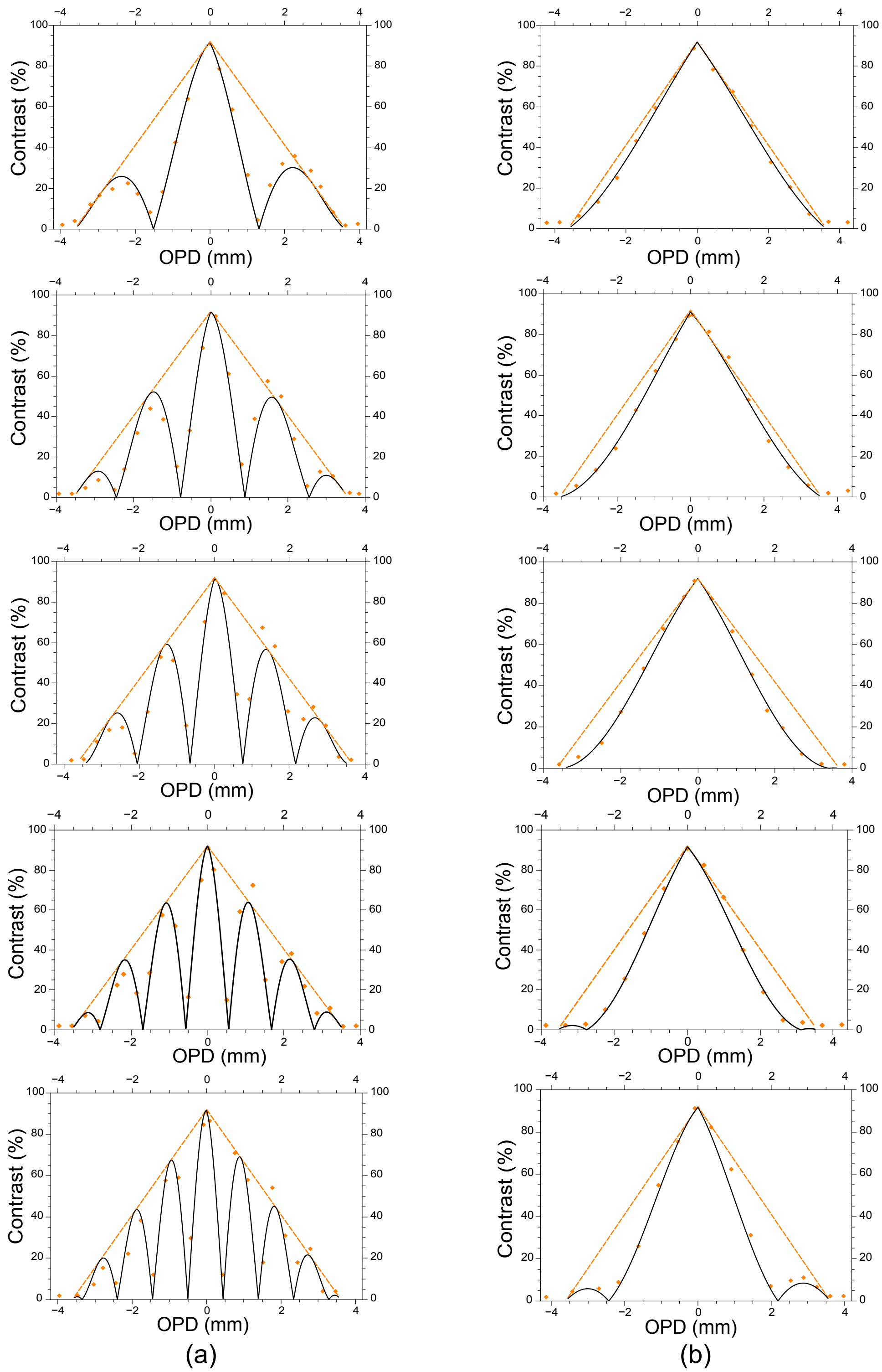

Fig. 10. Measured contrast for different frequency gap between the two pump frequencies (from top to bottom : 132.5 GHz, 212 GHz, 265.1 GHz, 318.1 GHz and 397.8 GHz). (a) Experimental fringe contrast versus the OPD applied on the infrared stage. (b) Experimental fringe contrast versus the OPD applied on the visible stage. In both cases the black curve represents the best theoretical fit of the experimental points.

#244263 Received 3 Jul 2015; revised 20 Aug 2015; accepted 21 Aug 2015; published 21 Sep 2015
© 2015 OSA

Table 1. Experimental spectral compression factor and relative error with the theoretical compression factor.

$\Delta\nu_p$ **(GHz)**	132.5	212.0	265.1	318.1	397.8
$L_{B_{IR}}$ **(mm)**	2.8	1.7	1.4	1.1	1.0
$L_{B_{VIS}}$ **(mm)**	11.3	8.9	7.0	5.9	4.6
ρ_{exp} **(mm)**	4.0	5.2	5.0	5.4	4.6
Relative error (%)	17	8	4	13	4

nificant error on the experimental compression factor ρ_{exp} that can explain the high values of relative error. This assertion can be confirmed by studying the dispersion of the terms $L_{B_{IR}}\Delta\nu_p$ and $L_{B_{VIS}}\Delta\nu_p$ for the different measurements since these terms are constant regardless spacing between pumps. The relative standard deviation is 4.8 % in infrared domain and 9.2 % in visible domain confirming that the fit parameters of visible contrast are less accurate.

5. Conclusion

In this paper, we have experimentally studied the spectral filtering effect on the temporal coherence behavior of a broadband infrared source upconverted by a pump spectral doublet in a PPLN crystal. The coherence properties of the converted field have been investigated with a Mach-Zehnder interferometer. While each sample of the infrared source is merely transposed in the visible domain without changing its frequency width, we have shown that the converted samples move closer to each other. This results in a modification of the coherence properties of the converted wave.

We have led this experimental study in a simple case with a dual-line pump source to understand the involved phenomena. In a next study, we plan to convert a broadband infrared source using a frequency comb with more than two lines. Moreover, within the frame of low flux detection, it will be necessary to analyze the noise behavior when many SFG processes simultaneously occur in a same crystal.

Acknowledgments

This work has been financially supported by the Centre National d'Études Spatiales (CNES). Our thanks go to A. Dexet for the development and his advice for all the specific mechanical components.